Received September 30, 2020, accepted October 22, 2020, date of publication October 26, 2020, date of current version November 6, 2020.

Digital Object Identifier 10.1109/ACCESS.2020.3033582

Determination of Moisture Content of Single Maize Seed by Using Long-Wave Near-Infrared Hyperspectral Imaging (LWNIR) Coupled With UVE-SPA Combination Variable Selection Method

ZHELI WANG[1,2], YIFEI ZHANG[1], SHUXIANG FAN[2], YINGLAN JIANG[1], AND JIANGBO LI[1,2]

[1]College of Mechanical and Electrical Engineering, Shihezi University, Shihezi 832003, China
[2]Beijing Research Center of Intelligent Equipment for Agriculture, Beijing 100097, China

Corresponding authors: Yinglan Jiang (shz-jyl@163.com) and Jiangbo Li (jbli2011@163.com)

This work was supported in part by the National Key Research and Development Program of China under Grant 2018YFD0101004, in part by the National Natural Science Foundation of China under Grant 31801262 and Grant 31972152, and in part by the Beijing Talents Foundation under Grant 2018000021223ZK06.

ABSTRACT Moisture content (MC) is one of the important factors to assess the quality of maize seeds. In this study, the feasibility of using long-wave near infrared (LWNIR) hyperspectral imaging (HSI) technique with the spectral range of 930-2548 nm for predicting MC of single maize seeds was observed. The averaged spectra extracted from whole and centroid regions in the embryo side of single maize seeds were pretreated by Savizky-Golay smoothing and first derivative (SG-D1). A combination of uninformative variable elimination (UVE) and successive projections algorithm (SPA) was proposed to select feature wavelengths (variables) from LWNIR hyperspectral data. The quantitative relationship between feature wavelengths and MC was established by partial least square (PLSR) and least square-support vector machine (LS-SVM), respectively. Results illustrated that the UVE-SPA-LS-SVM model established based on spectra of centroid region obtained the best performance for MC detection of the single maize seeds. The correlation coefficient of prediction (R_{pre}) and root mean square error of prediction (RMSEP) were 0.9325 and 1.2109, respectively. Finally, MC distribution of single maize seed was visualized by pseudo-color map. This study showed LWNIR HSI technique was feasible to measure MC of single maize seeds and a robust and accurate model could be established based on UVE-SPA-LS-SVM method with the spectra of centroid regions.

INDEX TERMS Maize seeds, moisture content detection, hyperspectral imaging, quantitative model establishment, moisture content visualization.

I. INTRODUCTION

Maize is an important source of energy and also one of the main cereals in the world [1]. The quality determination of maize seeds is vital to improve the maize's yield and quality. Moisture content (MC) is one of the critical factors to assess seeds quality. It directly affects the storage [2], [3]. During storage, high moisture levels will accelerate respiration, thus, the excessive water and heat can be produced, which may cause seeds to be infected by some fungi [4], [5]. Some researchers showed the best time to harvest maize is when MC is 21%-43% [6], [7]. Therefore, determination of MC of maize seeds is an indispensable step to ensure the quality of maize seeds. Besides, the MC detection of single seed is helpful to increase the uniformity and purity of seeds [8]. Usually, the methods used to detect the MC of agricultural products can be divided into two types of direct methods and indirect methods. The former mainly contains drying and Karl Fischer methods [9]. However, the process is time-consuming and destructive. The latter includes capacitance, conductance, and microwave methods [10]. These methods could achieve the rapid and nondestructive MC determination. However, the accuracy is limited and the MC detection of single seed is difficult. Hence, it is very meaningful to find a rapid, low cost, non-pollution and non-destructive method for MC detection of single maize seed.

In the past 20 years, some traditional non-destructive test technologies, such as near-infrared (NIR) spectroscopy and

The associate editor coordinating the review of this manuscript and approving it for publication was Qiangqiang Yuan.

the machine vision, have been widely used for quality detection in agricultural products and foods due to the low cost and fast detection speed [11], [12]. Recently, NIR spectroscopy has been used to determine the MC of meat [13], [14], fruit [15], [16] and other agricultural products [17], [18]. This technology also has been applied to detect MC of seeds [19]. Zhu, Chen, Wu *et al.* [20] developed the model to detect the moisture of soybeans based on NIR spectroscopy with the determination coefficient (R^2) of 0.966. Makky *et al.* [21] establish NIR spectral models for fast and nondestructive determination of moisture of two types of rice. The results indicated that MC of paddy grains can be effectively identified by using the spectral data of 1000-2500 nm. Although NIR spectroscopy has the potential to detect MC of seeds, it might not be the best choice for robust MC assessment. The main reason is that traditional NIR technology can only be used to analyze spectral data from local position of samples [22]. Moreover, the specialized NIR spectroscopy system needs to be developed for quality detection of a single seed. In fact, the development of this type of system is very difficult because the size of seeds is usually very small. Thus, the traditional NIR technology may not suit for MC determination of single seeds. As for the machine vision technique, it can only detect the external characteristics of seeds such as size, color and cracking [23]. Therefore, machine vision technology is not suitable for MC detection of seeds.

Hyperspectral imaging (HSI) can integrate traditional image and spectrum to provide information on the spatial and spectral features of an object [24]. Compared with NIR spectroscopy and machine vision, HSI can collect the spectral information of whole seed sample, which is helpful to obtain the more robust detection results in the assessment of MC of seeds [25], [26]. In recent years, HSI technology has been widely used to detect quality of many agricultural products such as meat [27], [28], fruit [29], vegetables [30] and nut [31]. In terms of MC detection of seeds, Lu *et al.* [32] applied HSI to detect MC of rich seeds successfully research showed that the MC detection of single seeds is feasible by using HIS technique. Xu *et al.* [22] used two HSI systems with the wavelength ranges of 400-1000 and 1050-2500 nm to detect the MC of cucumber seeds, respectively. The result indicated that the spectral region of 1050-2500 was more suitable for MC determination, and the spatial distribution of the MC of seeds could be visualized by hyperspectral images. Zhang and Guo [33] used Vis/NIR and NIR HSI systems to detect the MC of maize seeds based on the average spectra extracted from the whole seed region and centroid region on two sides of maize seeds, respectively. The results showed that the average NIR spectra collected from the centroid region had better performance. However, it is arduous and time-consuming to collect the average spectra of two sides of maize seeds, and it is also difficult to simultaneously obtain hyperspectral images of two sides of maize seeds in actual application. Besides, in the above researches, partial least squares regression (PLSR) model was established for MC determination of seeds. Although these studies have proved that the linear model has good performance in MC prediction of seeds. However, there may be some other factors (such as seed color, texture and stray light), which may have a nonlinear relationship with MC of seeds. Therefore, the establishment and analysis of nonlinear models is also very meaningful for MC assessment of seeds, especially seed quality analysis based on hyperspectral images. In this study, LWNIR hyperspectral imaging system was used to obtain spectral images and spectra from whole seed region and centroid region on the embryo side of maize seeds were extracted to establish the linear and nonlinear models for MC detection of single maize seed.

In general, hyperspectral image contains a great deal of grayscale sub-images [34]. So, the average spectrum extracted from each hyperspectral image also includes many wavelengths (variables). Thus, the full-spectrum data may exist multicollinearity and redundancy information [35]. Therefore, it is important to remove or reduce these useless variables before constructing a model based on suitable variables selection algorithms. The uninformative variable elimination (UVE) is an effective variable selection method to eliminate the useless variables [36]. However, the UVE only eliminates the non-information variables in the original spectra. Some collinear information may always exist in the remaining variables [37]. Therefore, in this study, the successive projection algorithm (SPA), a common variable selection algorithm, was used to select the variables with the minimum of collinearity is further used to optimize variables obtained from UVE algorithm [38], [39].

The main objectives of this article were: (1) to collect the LWNIR hyperspectral images of maize seeds (embryo side)and separately extract the average spectra from whole seed region and centroid region; (2) to select feature variables that were the most informative for determination of MC of seeds by variable selection algorithms of UVE and SPA; (3) to build the partial least squares regression (PLSR)linear models and least square-support vector machine (LS-SVM) nonlinear models based on feature variables for MC detection; and (4) to visualize the spatial distribution of MC of single maize seeds.

II. MATERIALS AND METHODS

A. MATERIALS

'Zhengdan 958' variety maize seeds were obtained from local seed market (Beijing, China). A total of 289 single seed samples were used in this study. In order to increase the MC gradient, samples were divided into 4 groups, and each group was wrapped in moist gauze and stored at a standard experiment chamber (2 °C and 50% relative humidity).

Every 12 hours, a group of samples was taken from the experiment chamber and placed in the laboratory for 8 hours to reduce the influence of temperature. Then, samples were put onto black cardboards for image acquisition. Each sample was randomly divided into calibration set and prediction set according to the ratio of 3:1. Therefore, 216 single maize

seed samples were used as the calibration set to establish prediction models, and the rest 73 samples were used as prediction set to assess the performance of models.

B. HYPERSPECTRAL REFLECTANCE IMAGING SYSTEM AND IMAGE QCQUISITION

The hyperspectral reflectance images of all samples were acquired by using HSI system (shown in Fig.1) with the spectral range of 930-2548 nm. The system comprises five main parts: a imaging spectrograph (ImSpector N25E, Spectral Imaging Ltd, Oulu, Finland), two 150 W halogen area light sources, a 320 × 256 CCD camera (Xeva-2.5-320, Xenics Ltd, Belgium), a motorized positioning sample table (EZHR17EN, AllMotion, Inc., USA) driven by a stepping motor, and a computer (Dell OPTIPLEX 990, Intel (R) Core (TM) i5-2400 CPU at 3.10 GHZ) with a SpectraCube data acquisition software and sample table control software (Isuzu Optics Corp., Taiwan). In order to avoid the interference of stray light, the system was placed in an inspection chamber painted with black matte ink. For acquiring the high-quality image and avoiding the influence of the thermal effect of the light source, some image acquisition parameters need to be set firstly and collect the hyperspectral images as fast as we can. In this study, the distance between CCD camera and samples was adjusted to 400 mm. The distance between the two light sources was 550 mm, and the angle between each light source and the horizontal plane was 45°. The moving speed of mechanical platform and the exposure time of the CCD camera were set as 43 mm/s and 2 ms, respectively. The spectrograph has a fixed-size internal slit to define a field of view (FOV) for the spatial line (horizontal pixel direction) and collected spectral images at 6.32 nm intervals within a wavelength range of 930–2548 nm. Therefore,

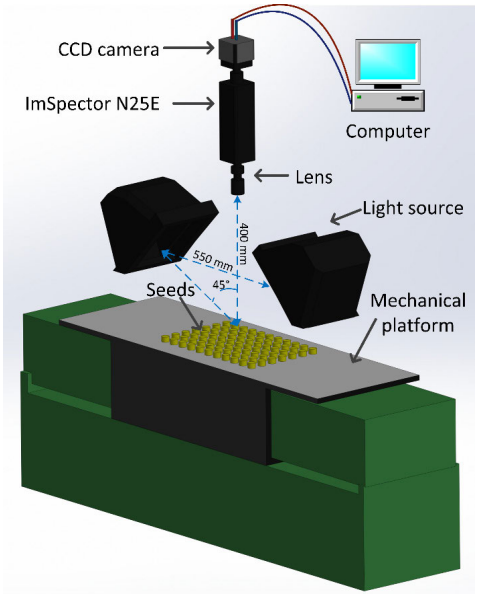

FIGURE 1. Hyperspectral imaging system.

for the acquired hyperspectral images, each image contains 256 single wavelength images in the full-spectrum range. Note that each single seed sample was manually put onto platform and oriented with the seed side that contained the embryo toward the camera during the image acquisition.

Halogen lamps produce a spatial intensity variation in the plane of the scene and the dark current also exists in the CCD camera, which result in a large amount of noises for some bands with less light intensity. Therefore, the acquired hyperspectral images (R_o) were first corrected with white (R_w) and dark (R_b) references before further data processing and analysis [40]. A white diffuse reflectance board with a 99% reflection efficiency (Spectralon SRT-99-100, Labsphere Inc., North Sutton, NH, USA) was used to obtain a typical white reference image. This dark current image with 0% reflectance was collected by turning off the lamps and covering the lens with a black cap. The corrected image (R) was then calculated based on equation (1):

$$R = \frac{R_o - R_b}{R_w - R_b} \times 100\% \tag{1}$$

C. EXTRACTION AND PRETREATMENT OF SPECTRA OF REGIONS OF INTEREST

Before establishing the models, spectra of regions of interest (ROIs) of samples need to be extracted firstly. Specific steps are as follows: (1) creation of mask image. The maximum between-class method (also called OTSU), a classical method to obtain image binarization best treatment thresh, was applied to the grayscale image at 1098 nm to create a mask image. Note that image at 1098 nm was used because there is very obvious contrast between background and maize seeds region in the image; (2) Background segmentation. the mask image was multiplied by the grayscale images at each wavelength to remove the background; (3) Extraction of spectra. The average spectra from the whole region and single centroid region of embryo side of each seed were separately extracted for observing moisture content detection performance based on different regions of interest (ROIs). The function of 'bwlabel' and 'regionprops' was used to mark centroid in the mask image automatically. The size of each centroid region was 4 pixels × 4 pixels, the regions can collect the germ area of maize seeds as much as possible. In addition, if the size of centroid regions is small, the randomness of the data will be increase, if the size is large, the spectral information of endosperm area also be collected. Fig. 2 shows the flow chart for extracting spectral data of single maize seeds from hyperspectral image.

The original spectral data may contain some high-frequency random noise information that should be eliminated to improve the model's prediction performance [41]. In this study, processing methods including the savitzky-golay (SG) smoothing (window size: 15-point), standard normal variable (SNV), multiple scattering correction (MSC) and first derivative (D1) were applied to preprocess the spectral data.

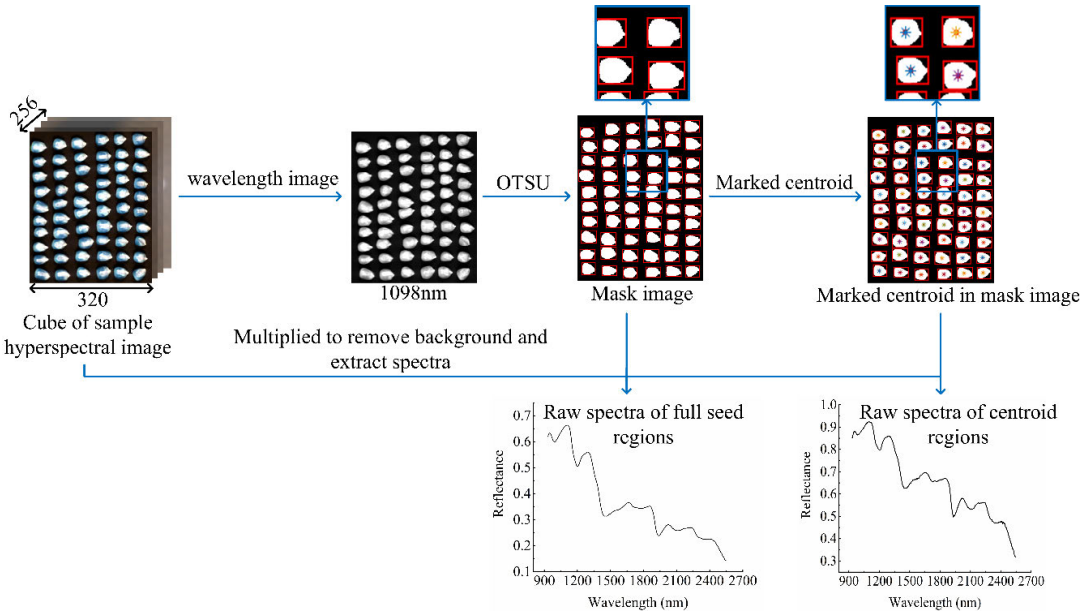

FIGURE 2. Flow chart for extraction the spectral data of single maize seeds.

D. REFERENCE MEASUREMENT

MC references of samples were measured immediately by using the gravimetric method after hyperspectral image was acquired. The seed samples were put in the oven at 135 °C for 48 h. High temperature and dry environment are beneficial for dehydration. Weight of samples was measured by an analytical balance (LS220A, Precisa, Switzerland) before and after drying. The MC calculation equation was as follows:

$$MC = \frac{W0 - W1}{W0} \times 100\% \quad (2)$$

where MC represents the moisture content of samples, W_0 and W_1 represent the weight of samples before and after drying, respectively. Table 1 shows the statistical values of MC of all maize seed samples. The range of MC values for all samples was 9.12-32.91% with average of 15.57% and standard deviation of 3.12%. Specifically, the distribution range of reference values was 9.12-32.91% for calibration set and was 10.93-25.28% for prediction set, respectively. The MC values in the sample sets covered a large range, and the MC range of the calibration set is larger than that of the prediction set. These features were helpful to establish a robust model.

E. VARIABLES SELECTION METHODS

Two complementary wavelength selection strategies may achieve a superimposed effect when combined together [29]. In this study, the uninformative variable elimination (UVE) and successive projections algorithm (SPA) were combined to select the feature wavelengths for optimizing the model fit and improving the prediction performance. Specifically, UVE was first used to obtain a group of potential wavelengths related to MC of seeds. Then, SPA was utilized to select the most effective variable subset from those identified potential wavelengths. The UVE and SPA are two efficient spectral variable selection methods that have been used to facilitate high-performance calibration model development by selecting the most informative variables [42].

TABLE 1. The statistic of moisture content of maize seeds in calibration and prediction sets.

Sample set	No. of samples	Max/%	Min/%	Average/%	SD
Total	289	32.91	9.12	15.57	3.13
Prediction set	73	26.48	11.16	15.72	3.18
Calibration set	216	32.91	9.12	15.52	3.11

Abbreviations: Max: maximal moisture content of maize seeds; Min: minimal moisture content of maize seeds; SD: standard deviation.

The UVE algorithm, proposed by Centner *et al.* [43], is a powerful and widely used technique for analyzing complex spectral problems based on partial least squares (PLS) regression coefficient $\boldsymbol{b}$. For performing UVE, a random matrix $\mathbf{R}(n, p)$ first need to be added to the spectral matrix $\mathbf{X}(n, p)$ to create a new matrix $\mathbf{X}(n, 2p)$. Then, the PLSR model is built with leave-one-out method according to $\mathbf{XR}(n, 2p)$. Then, the PLS regression coefficients matrix $\mathbf{B}(n, 2p)$ is calculated through a leave-one-out validation by using $\mathbf{XR}$. The standard deviation $\mathbf{s}(1, 2p)$ and the average value $\mathbf{m}(1, 2p)$ of each column vector of the matrix $\mathbf{B}(n, 2p)$ are calculated, and then Ci=(mi)/(si), i=1, 2…., 2p. In the $[p + 1, 2p]$ interval, the maximum absolute value is Cmax = max(abs(c)). Lastly, the variables, corresponding to c(i) < Cmax of matrix $\mathbf{X}$ in the $[1, p]$ interval, should be removed and the remained variables are the feature variables selected by UVE.

SPA that is proposed by Araújo *et al.* [44] can be used to obtain those wavelengths with minimal collinearity in the selected wavelengths by UVE. SPA is a forward selection method for multivariate calibration. The principle of variable selection by SPA is that the new variable selected is the one among all the remaining variables, which has the maximum projection value on the orthogonal subspace of the previous selected variable. The optimal initial variable and number of variables can be determined on the basis of the smallest root mean square error of validation (RMSEP) in validation set of MLR calibration (Araújo *et al.*, 2001). A UVE-SPA combination algorithm appears to be rarely used for effective wavelength selection of seed samples in the LWNIR spectral region. A graphical user interface for the SPA (GUI_SPA) is available at http://www.ele.ita.br/∼kawakami/spa/.

F. ESTABLISHMENT OF MODELS

PLSR is a powerful method to describe the linear relationship between the spectral data **X** and response variables **Y**. PLSR algorithm can eliminate multicollinearity and solve the problem that the number of samples is less than the number of variables [45]. Therefore, it is suitable to establish a calibration model for MC detection in maize seeds in this study. The most critical step in building a PLSR model is to determine the number of latent variables (LVs). The leave-one-out cross-validation strategy is commonly used to obtain the optimal number of LVs, however, this method only changes one sample in each cross-validation. Therefore, it could result in the predictive performance over-optimistic [46]. In this study, the 10-fold cross-validation is used to determine the optimal number of LVs until the mean square error of cross-validation (RMSECV) reaches a minimum.

LS-SVM is an evolutionary version of the standard support vector machines (SVM), which involves equality instead of inequality constraints and works with the least square cost function [47]. Moreover, unlike PLSR, it not only could deal with linear problems, but also nonlinear problems. LS-SVM has been widely used as a classical nonlinear modeling method to establish a regression model for quantitative and qualitative analysis [48]–[50]. A typical LS-SVM model can be expressed as

$$y(x) = \sum_{k=1}^{N} \alpha_k K(x, x_k) + b \tag{3}$$

where $K(x, x_k)$ is the kernel function, x_k is the input vector, α_k is the Lagrange multiplier, and b is the bias. The radial basis function (RBF) that could handle the nonlinear relationship between the spectra and MC is used as the kernel function. It is defined as follows:

$$K(x,x_k) = exp(-//x_k - x//^2/(2\sigma^2)) \tag{4}$$

In LS-SVM modeling based on RBF kernel, two parameters both *gamma* (γ) and *sig2* (σ^2) need to be calculated. Usually, the optimal combination of (γ, σ^2) is determined by a two-step grid search technique based on the 10-fold cross-validation of the calibration set. The first step grid search was applied for a crude search with a large step size and the second step was applied for the specified search with a small step size. After the process of grid search, the optimal combination of (γ, σ^2) would be achieved for the LS-SVM models.

The predictive performance of all models is evaluated by correlation coefficient (R_{cal}) and root mean square error of calibration (RMSEC) for calibration set and by correlation coefficient (R_{pre}) and root mean square error of prediction (RMSEP) for prediction set, respectively four parameters. Generally speaking, a good model has a relatively higher R value and lower RMSE value. The RMSEC and RMSEP are defined by the following equation (5) and (6):

$$RMSEC = \sqrt{\frac{1}{nc}\sum_{i=1}^{nc}(Yi - yi)^2} \tag{5}$$

$$RMSEP = \sqrt{\frac{1}{np}\sum_{i=1}^{np}(Yi - yi)^2} \tag{6}$$

where Y_i and y_i are the predicted value and measured valued of the i-th observation in calibration and prediction set, respectively. n_c and n_p are the number of observations in the calibration and prediction set, respectively.

The R is defined as follows:

$$R = \sqrt{1 - \frac{\sum_{i=1}^{n}(yi - Yi)^2}{\sum_{i=1}^{n}(yi - \bar{y})^2}} \tag{7}$$

where $\bar{y}$ is the mean value of the calibration or prediction set; Y_i and y_i are the predicted value and measured valued of the i-th observation in calibration and prediction set, respectively; n is the number of samples in the calibration set or prediction set.

G. VISUALIZATION OF MC OF DISTRIBUTION

In hyperspectral images, each pixel contains a spectrum, which makes it possible to visualize the MC distribution of seeds. In order to observe the MC distribution in maize seeds, the spectrum of each pixel was used as input of the established optimal model to calculate the MC value of the corresponding pixel in the hyperspectral image. Thus, the hyperspectral image was translated into a MC value image [51], [52]. MC distribution map was then created by pseudo color transformation with a color bar. By visualization processing, the MC distribution in different areas of each maize seed can be observed intuitively.

III. RSEULTS AND DISCUSSION

A. OVERVIEW OF SPECTRA

Two types of spectra, obtained from the whole regions and centroid regions of seeds, were used in this study. These two types of raw reflectance spectra in the wavelength range

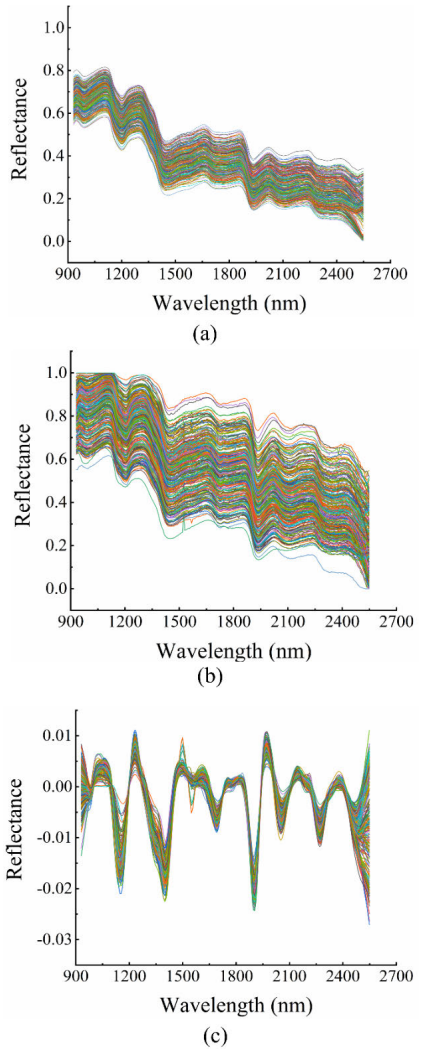

FIGURE 3. The NIR hyperspectral spectra of maize seeds. (a) the raw reflectance spectra of whole regions. (b) the raw reflectance spectra of centroid regions. (c) the pretreatment spectra of centroid regions (savitzky-golay (SG) smoothing and first derivative).

of 930-2548 nm are shown in Fig. 3(a) and (b), respectively. it can be found that the trends of all spectral curves are similar, but the reflectance values of centroid regions are higher than ones of whole regions. The reason is that the centroid region of each seeds located in its embryo region. In terms of maize seeds, the color of embryo region is white or light and that of endosperm region is yellow or dark. Four absorption peaks around at 960, 1200, 1450 and 1950 nm can be observed from Fig. 3(a) and (b). The absorption peak around at 960 nm may associate with the second overtone of the O-H stretching, which exists in carbohydrates and water [53]. The clear absorption peak about at 1200 nm might be contributed by the second overtone of the C-H stretching, which associates with the carbohydrates [54]. The absorption peak about at 1450 nm is related to the first overtone of O-H stretching, which caused by water [55]. In addition, there is an absorption peak about at 1950 nm which is inconspicuous and mainly caused by the combination tone of water [56].

B. DECISION ON ROI AND PRETREATMENT METHODS

To determine which type of ROI is more suitable for MC prediction of maize seeds, the average spectra (raw and pre-processed spectra by SG combined with SNV, MSC, and first derivative) extracted from whole region and centroid region were used as input to establish PLSR and LS-SVM models, respectively. All models were established based on the 10-folds cross-validation, and the prediction results are shown in Table 2. It can be found that the models established based on the spectra of centroid region obtained better MC prediction accuracy than the models established based on the spectra of whole seed region in all models including linear or nonlinear models. For instance, R_{CV} and RMSECV of PLSR model built by the raw average spectra of centroid region were 0.9258 and 1.1776%, respectively. In contrast, R_{CV} and RMSECV were 0.9055 and 1.3218% for model established by the raw average spectra extracted from whole seed region. Further comparison, it can also be seen clearly that models established by the SG-D1 preprocessing spectra of centroid region have better prediction accuracy with $R_{CV=}0.93$ and RMSECV = 1.17% for PLSR model and R_{CV} = 0.93 and RMSECV=1.11% for LS-SVM model. Therefore, the SG-D1 preprocessing spectra extracted from centroid region were used for the subsequent analysis.

TABLE 2. The prediction results of moisture content of maize seeds by PLSR and LS-SVM models with different spectra of ROIs.

Methods	Preprocessing methods	ROIs	R_{CV}	RMSECV/%
PLSR	None	Whole seeds	0.91	1.32
		Centroid	0.92	1.18
	SG-MSC	Whole seeds	0.90	1.34
		Centroid	0.92	1.21
	SG-D1	Whole seeds	0.90	1.33
		Centroid	0.92	1.17
	SG-SNV	Whole seeds	0.90	1.34
		Centroid	0.92	1.22
LS-SVM	None	Whole seeds	0.91	1.26
		Centroid	0.92	1.14
	SG-MSC	Whole seeds	0.90	1.29
		Centroid	0.91	1.14
	SG-D1	Whole seeds	0.90	1.24
		Centroid	0.93	1.11
	SG-SNV	Whole seeds	0.91	1.29
		Centroid	0.91	1.16

Abbreviations: PLSR: partial least squares regression; LS-SVM: least squares-support vector machine; Rcv: correlation coefficient of cross-validation; RMSECV: root mean square error of cross validation; SG-MSC: savitzky-golay smoothing combined with multiple scatter correction; SG-D1: savitzky-golay smoothing combined with first derivative; SG-SNV: savitzky-golay smoothing combined with standard normal variable.

C. VARIABLE SELECTION BASED ON UVE

The UVE algorithm was used to eliminate useless information in the original data. In the UVE process, the feature variables are determined by the number of latent variables (LVs), and the number of LVs was determined by the smallest RMSECV. Fig. 4(a) shows the change relationship between the RMSECV values and LVs number of 1-20. As shown in Fig. 4(a), the RMSECV obtained the optimal value when the number of LVs was equal to 10. Thus, the UVE with 10 LVs was used to calculate the stability value of each wavelength in full spectra. Fig. 4(b) indicates show the stability of each variable for MC analysis of maize seed by UVE. In the figure, the dot lines represent the cutoffs (threshold values). The variables between dot lines are treated as the uninformative variables to be eliminated, and the rest variables will be used to establish the PLSR and LS-SVM calibration model or for further analysis. Finally, 93 variables were selected by UVE.

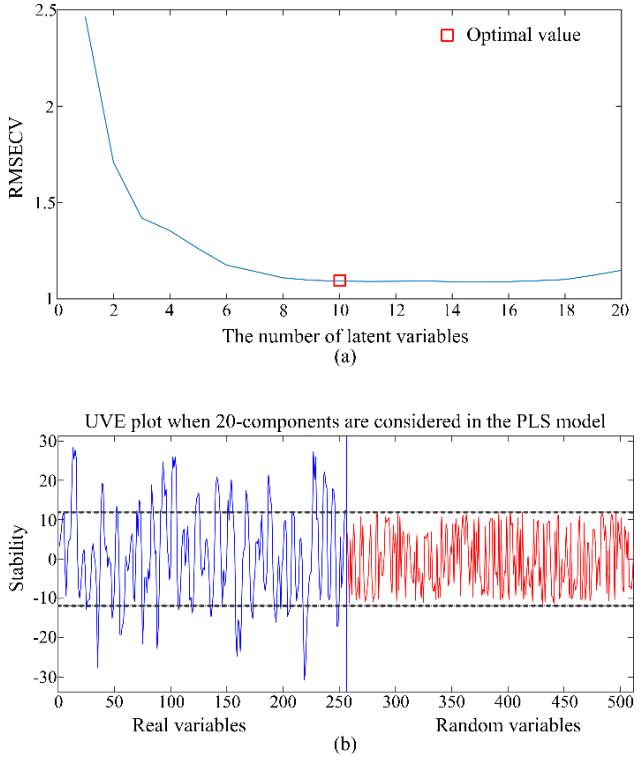

FIGURE 4. Feature variable selection by UVE. (b) stability distribution of each variable. (a) The change curve of RMSECV by UVE algorithm. (b) Feature wavelengths screened by the UVE algorithm.

D. VARIABLE SELECTION BASED ON SPA

Although the number of variables decreased from 256 to 93 by UVE, some collinear variables which contain a large number of redundant information are still existent because UVE method only can eliminate the uninformative variables in the spectra data. Moreover, in terms of practical application, a more effective, simple, and fast model is always desired. Therefore, 93 variables selected by UVE were further analyzed by SPA algorithm to optimize models. 93 variables were used as input of SPA. In the process of SPA, a SPA-MLR procedure was applied for the calculation of a sequence of RMSEV values using the selected variables subsets. This process confirmed the optimal number of selected effective wavelengths with an optimal RMSEV value. Fig. 5 shows the wavelength selection results by SPA. Fig. 5(a) shows the RMSE screen plots for the number of variables selected by SPA. It can be clearly seen that the RMSE values have a dramatic drop when the number of variables changes from 1 to 10. Subsequently there was a moderate change. The RMSE of the model reaches the optimal one (RMSE=1.0764) when 18 variables were selected (square symbol in Fig. 5(a)). However, the feature variables could not be directly obtained from Fig. 5(a). Fig. 5(b) shows the selected 18 variables (solid square symbol) for prediction of MC. These variables include 1005.95, 1079.57, 1141.77, 1222.82, 1272.81, 1360.47, 1391.84, 1511.32, 1555.45, 1580.70, 1593.33, 1707.23, 1872.47, 2115.49, 2147.60, 2308.63, 2425.05 and 2470.43 nm, respectively. It can be found that these feature variables were mainly concentrated in NIR region of 1000-1900 nm. According to analysis of 3.1 section, these feature variables relate to H_2O or carbohydrates, further demonstrating the effectiveness of these wavelengths for MC prediction of maize seeds.

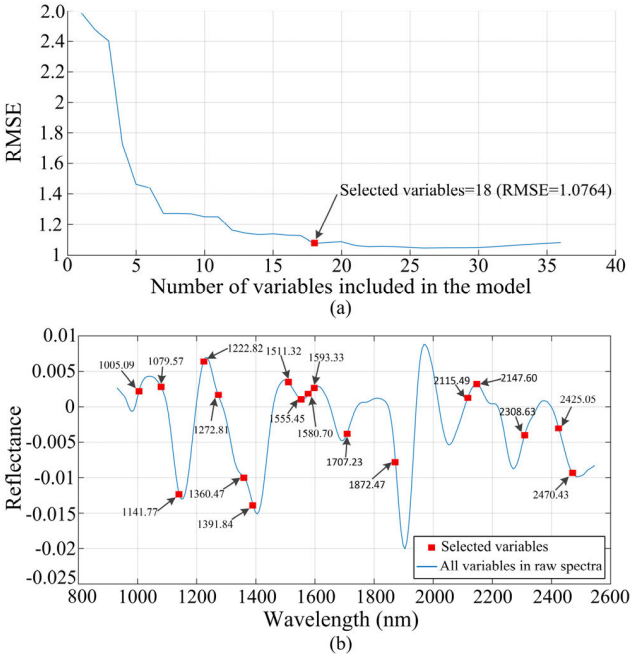

FIGURE 5. Feature variable selection by SPA. (a) RMSE plots obtained for MC of maize by SPA. (b) The selected variables for MC of maize by SPA.

E. MC PREDICTION RESULT AND ANALYSIS

Two types of models including linear PLSR and nonlinear LS-SVM were established for MC analysis of maize seeds based on different inputs including full-spectrum (256 wavelengths) and feature variables (93 wavelengths by UVE

TABLE 3. The prediction results of moisture content of maize seeds by PLSR and LS-SVM models with different input variables.

Methods	Preprocessing methods	No. of variables	Calibration set		Prediction set	
			R_{cal}	RMSEC/%	R_{pre}	RMSEP/%
PLSR	None	256	0.95	0.98	0.91	1.35
	UVE	93	0.95	0.96	0.90	1.36
	UVE-SPA	18	0.95	0.98	0.91	1. 32
LS-SVM	None	256	0.97	0.81	0.92	1.31
	UVE	93	0.96	0.86	0.92	1.34
	UVE-SPA	18	0.96	0.87	0.93	1.21

Abbreviations: PLSR: partial least squares regression; LS-SVM: least squares-support vector machine; UVE: uninformative variable elimination algorithm; UVE-SPA: uninformative variable elimination algorithm combined with successive projections algorithm; RMSEC: root mean square error of calibration; RMSEP: root mean square error of prediction; Rcal: correlation coefficient of calibration set; Rpre: correlation coefficient of prediction set.

and 18 wavelengths by UVE-SPA). For LS-SVM models, the optimal combinations of (γ, σ^2) were (316.6688, 0.2418), $(1.3613 \times 10^3, 0.0095)$ and $(9.0923 \times 10^3, 0.0015)$for full-spectrum-LS-SVM model, UVE-LS-SVM model and UVE-SPA-LS-SVM model, respectively. Table 3 shows the MC prediction results by different models. Based on full spectral data, R_{pre} and RMSEP of PLSR model were 0.9056 and 1.3502, and R_{pre} and RMSEP of LS-SVM model were 0.9233 and 1.3154, indicating that full spectral data can be used to predict MC of maize seeds. Compared with full-spectrum models, models based on UVE and UVE-SPA also obtained similar or better results. These results showed that UVE and UVE-SPA methods were a very useful tool for selecting effective variables for MC detection of maize seeds. Comparing full-spectrum models, RMSEP values of PLSR and LS-SVM were slightly lower although the UVE-PLSR and UVE-LS-SVM models used less variables. RMSEP values of UVE-PLSR and UVE-LS-SVM models were 1.3582 and 1.3437, respectively. In all linear models or nonlinear models, models established based on 18 variables selected by UVE-SPA gave more accurate MC prediction results with RMSEP=1. 3202 for UVE-SPA-PLSR and RMSEP=1.2109 for UVE-SPA-LS-SVM, respectively. The result showed that the proposed UVE-SPA combination method was useful for this study.

Further comparing between PLSR and LS-SVM models, it can be seen from Table 3 that all LS-SVM models obtained better results for calibration and prediction sets when the same variables were used as input. The reason could be that LS-SVM model can more effectively process nonlinear relationship between spectra and MC of seeds. In fact, some latent nonlinear information (texture information and color information of seeds) related to MC prediction may still exist in the spectra. For UVE-SPA-LS-SVM model, A comprehensive comparison of Tables 3 indicated that UVE-SPA-LS-SVM model was optimal for MC prediction of maize seeds with accuracy of $R_{cal} = 0.96$ and RMSEC = 0.87 for calibration set and $R_{pre} = 0.93$ and RMSEP = 1.21 for prediction set among all the models established in this study. Therefore, UVE-SPA-LS-SVM model could be considered as an excellent model for detecting MC of maize seeds. Fig. 6 shows the scatter plots of predicted versus measured values for MC prediction by the UVE-SPA-LS-SVM model.

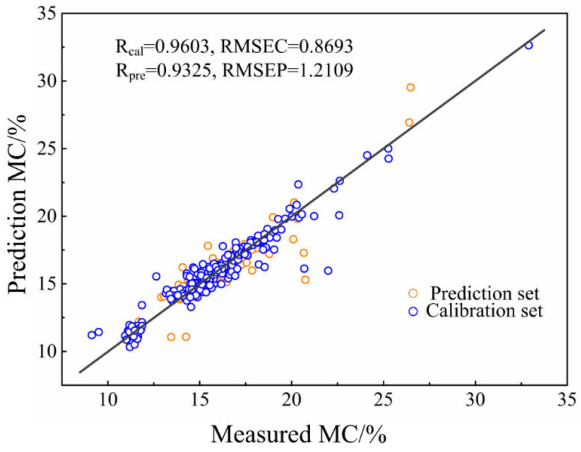

FIGURE 6. Measured vs. prediction values for MC prediction by the UVE-SPA-LS-SVM model.

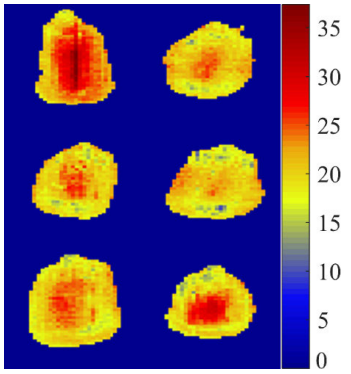

FIGURE 7. Visualization of MC of maize seeds in the hyperspectral image.

F. VISUALIZATION OF MC

Hyperspectral image contains spectral and spatial information, which makes it possible to visualize the moisture content of maize seeds. The optimal LS-SVM model (UVE-SPA-LS-SVM) based on 18 variables which were selected by UVE-SPA was used to predict MC value of each pixel in hyperspectral image and map them with pseudo color to better understand the water distribution in maize seeds. The visualization of MC in some typical maize seeds was shown in Fig. 7. In this figure, the different color on seeds represents

different MC, and the color from blue to red corresponds to the MC value from low to high. It can be seen from Fig. 7 that the MC of embryo regions was significantly higher than other regions because the embryo regions of maize seeds store lots of water. This MC visualization result is consistent with the analysis results from Table 2, that is, the spectra from centroid region which is usually located in embryo region of seeds have better MC prediction performance.

IV. CONCLUSION

In this study, the long-wave NIR hyperspectral imaging (930-2548 nm) coupled with UVE-SPA combination variable selection algorithm and LS-SVM model was successfully utilized for determining the MC of maize seeds. The spectra of centroid region and whole region of seeds were separately used to establish models and results showed that centroid region is more suitable for establishment of MC prediction models. Further study indicated that CARS-SPA was a powerful combination way to select the most relevant wavelengths with least collinearity and redundancies. Only 18 effective wavelengths were extracted for MC prediction, which reduces the calculation time and increases model prediction performance. PLSR and LS-SVM models were built to predict MC. The results indicated that the UVE-SPA-LS-SVM model based on the 18 spectral variables of centroid regions achieved the best prediction performance with $R_{pre} = 0.93$ and RMSEP = 1.21. Based on UVE-SPA-LS-SVM model, the distribution map of MC was created to analyze the MC of each maize seed intuitively, and the visualization image also indicated that the spectra selected from centroid regions were more suitable for detecting MC of maize seeds. Overall, the results show that the newly proposed UVE-SPA-LS-SVM model combined with spectra of centroid regions could be applied as an alternative fast and accurate method for the determination of MC of single maize seed. Even so, the proposed method always needs to be further optimized by using a large number of maize seed samples for developing a more robust and accurate prediction model. In addition, the development of the fast-multispectral imaging system based on the 18 feature variables is also the focus of the next step.

REFERENCES

[1] P. J. Williams, P. Geladi, T. J. Britz, and M. Manley, "Investigation of fungal development in maize kernels using NIR hyperspectral imaging and multivariate data analysis," *J. Cereal Sci.*, vol. 55, no. 3, pp. 272–278, May 2012.

[2] Y.-Y. Lee, S. Rajametov, Y.-C. Kim, J.-Y. Yi, G.-A. Lee, J.-G. Gwak, E.-H. Son, and H.-J. Park, "Response of germination rate to variable drying conditions and moisture contents for storage of dehisced korean ginseng seeds," *Korean J. Plant Resour.*, vol. 29, no. 6, pp. 670–678, Dec. 2016.

[3] P. R. Rani, V. Chelladurai, D. S. Jayas, N. D. G. White, and C. V. Kavitha-Abirami, "Storage studies on pinto beans under different moisture contents and temperature regimes," *J. Stored Products Res.*, vol. 52, pp. 78–85, Jan. 2013.

[4] I. Niaz, S. Dawar, and U. Sitara, "Effect of different moisture and storage temperature on seed borne Mycoflora of maize," *Pakistan J. Botany*, vol. 43, no. 5, pp. 2639–2643, Oct. 2011.

[5] R. Wang, L. Liu, Y. Guo, X. He, and Q. Lu, "Effects of deterioration and mildewing on the quality of wheat seeds with different moisture contents during storage," *RSC Adv.*, vol. 10, no. 25, pp. 14581–14594, Apr. 2020.

[6] L. Dai, L. Wu, Q. Dong, Z. Zhang, N. Wu, Y. Song, S. Lu, and P. Wang, "Genome-wide association study of field grain drying rate after physiological maturity based on a resequencing approach in elite maize Germplasm," *Euphytica*, vol. 213, no. 8, p. 12, Aug. 2017.

[7] G. Zhou, D. Hao, L. Xue, G. Chen, H. Lu, Z. Zhang, M. Shi, X. Huang, and Y. Mao, "Genome-wide association study of kernel moisture content at harvest stage in maize," *Breeding Sci.*, vol. 68, no. 5, pp. 622–628, 2018.

[8] L. Esteve Agelet and C. R. Hurburgh, "Limitations and current applications of near infrared spectroscopy for single seed analysis," *Talanta*, vol. 121, pp. 288–299, Apr. 2014.

[9] E. Achata, C. Esquerre, C. O'Donnell, and A. Gowen, "A study on the application of near infrared hyperspectral chemical imaging for monitoring moisture content and water activity in low moisture systems," *Molecules*, vol. 20, no. 2, pp. 2611–2621, Feb. 2015.

[10] S. O. Nelson and S. Trabelsi, "Historical development of grain moisture measurement and other food quality sensing through electrical properties," *IEEE Instrum. Meas. Mag.*, vol. 19, no. 1, pp. 16–23, Feb. 2016.

[11] Z. M. Guo, M. M. Wang, A. A. Agyekum, J. Z. Wu, Q. S. Chen, M. Zuo, H. R. El-Seedi, F. F. Tao, J. Y. Shi, Q. Ouyang, and X. B. Zou, "Quantitative detection of apple watercore and soluble solids content by near infrared transmittance spectroscopy," *J. Food Eng.*, vol. 279, p. 10, Aug. 2020.

[12] H. S. El-Mesery, H. P. Mao, and A. Abomohra, "Applications of non-destructive technologies for agricultural and food products quality inspection," *Sensors*, vol. 19, no. 4, p. 23, Feb. 2019.

[13] A. Kartakoullis, J. Comaposada, A. Cruz-Carrión, X. Serra, and P. Gou, "Feasibility study of smartphone-based near infrared spectroscopy (NIRS) for salted minced meat composition diagnostics at different temperatures," *Food Chem.*, vol. 278, pp. 314–321, Apr. 2019.

[14] N. Prieto, O. Pawluczyk, M. E. R. Dugan, and J. L. Aalhus, "A review of the principles and applications of near-infrared spectroscopy to characterize meat, fat, and meat products," *Appl. Spectrosc.*, vol. 71, no. 7, pp. 1403–1426, Jul. 2017.

[15] C. Lee, J. J. Polari, K. E. Kramer, and S. C. Wang, "Near-infrared (NIR) spectrometry as a fast and reliable tool for fat and moisture analyses in olives," *ACS Omega*, vol. 3, no. 11, pp. 16081–16088, Nov. 2018.

[16] A. M. Alhamdan and A. Atia, "Non-destructive method to predict barhi dates quality at different stages of maturity utilising near-infrared (NIR) spectroscopy," *Int. J. Food Properties*, vol. 20, no. sup3, pp. S2950–S2959, Dec. 2017.

[17] O. C. Wokadala, C. Human, S. Willemse, and N. M. Emmambux, "Rapid non-destructive moisture content monitoring using a handheld portable Vis–NIR spectrophotometer during solar drying of mangoes (Mangifera indica L.)," *J. Food Meas. Characterization*, vol. 14, no. 2, pp. 790–798, Apr. 2020.

[18] G. B. Rossi and V. A. Lozano, "Simultaneous determination of quality parameters in yerba mate (Ilex paraguariensis) samples by application of near-infrared (NIR) spectroscopy and partial least squares (PLS)," *LWT*, vol. 126, May 2020, Art. no. 109290.

[19] L. Lin, Y. He, Z. T. Xiao, K. Zhao, T. Dong, and P. C. Nie, "Rapid-detection sensor for rice grain moisture based on NIR Spectroscopy," *Appl. Sci.-Basel*, vol. 9, no. 8, p. 13, Apr. 2019.

[20] Z. Zhu, S. Chen, X. Wu, C. Xing, and J. Yuan, "Determination of soybean routine quality parameters using near-infrared spectroscopy," *Food Sci. Nutrition*, vol. 6, no. 4, pp. 1109–1118, Jun. 2018.

[21] M. Makky, Santosa, R. E. Putri, and K. Nakano, "Determination of moisture content in rice using non-destructive short-wave near infrared spectroscopy," in *Proc. 2nd Int. Conf. Biosci. Med. Eng. (ICBME), Towards Innov. Res. Cross-Disciplinary Collaborations*, 2019, Art. no. 020014.

[22] Y. Xu, H. Zhang, C. Zhang, P. Wu, J. Li, Y. Xia, and S. Fan, "Rapid prediction and visualization of moisture content in single cucumber (Cucumis sativus L.) seed using hyperspectral imaging technology," *Infr. Phys. Technol.*, vol. 102, Nov. 2019, Art. no. 103034.

[23] J. B. Li, W. Q. Huang, and C. J. Zhao, "Machine vision technology for detecting the external defects of fruits—A review," *Imag. Sci. J.*, vol. 63, no. 5, pp. 241–251, Jun. 2015.

[24] L. S. Huang, H. S. Zhang, C. Ruan, W. J. Huang, T. G. Hu, and J. L. Zhao, "Detection of scab in wheat ears using in situ hyperspectral data and support vector machine optimized by genetic algorithm," *Int. J. Agricult. Biol. Eng.*, vol. 13, no. 2, pp. 182–188, Mar. 2020.

[25] Q. Liu, D. Zhou, S. Tu, H. Xiao, B. Zhang, Y. Sun, L. Pan, and K. Tu, "Quantitative visualization of fungal contamination in peach fruit using hyperspectral imaging," *Food Anal. Methods*, vol. 13, no. 6, pp. 1262–1270, Jun. 2020.
[26] H. Z. Jiang, F. N. Cheng, and M. H. Shi, "Rapid identification and visualization of jowl meat adulteration in pork using hyperspectral imaging," *Foods*, vol. 9, no. 2, p. 16, Feb. 2020.
[27] L. Kandpal, H. Lee, M. Kim, C. Mo, and B.-K. Cho, "Hyperspectral reflectance imaging technique for visualization of moisture distribution in cooked chicken breast," *Sensors*, vol. 13, no. 10, pp. 13289–13300, Sep. 2013.
[28] J.-H. Qu, D.-W. Sun, J.-H. Cheng, and H. Pu, "Mapping moisture contents in grass carp (ctenopharyngodon idella) slices under different freeze drying periods by vis-NIR hyperspectral imaging," *LWT*, vol. 75, pp. 529–536, Jan. 2017.
[29] H. Zhang, B. Zhan, F. Pan, and W. Luo, "Determination of soluble solids content in oranges using visible and near infrared full transmittance hyperspectral imaging with comparative analysis of models," *Postharvest Biol. Technol.*, vol. 163, May 2020, Art. no. 111148.
[30] Z. Du, X. Zeng, X. Li, X. Ding, J. Cao, and W. Jiang, "Recent advances in imaging techniques for bruise detection in fruits and vegetables," *Trends Food Sci. Technol.*, vol. 99, pp. 133–141, May 2020.
[31] J. Sun, X. Shi, H. Zhang, L. Xia, Y. Guo, and X. Sun, "Detection of moisture content in peanut kernels using hyperspectral imaging technology coupled with chemometrics," *J. Food Process Eng.*, vol. 42, no. 7, p. 10, Nov. 2019.
[32] B. Lu, J. Sun, N. Yang, X. Wu, X. Zhou, and J. Shen, "Quantitative detection of moisture content in rice seeds based on hyperspectral technique," *J. Food Process Eng.*, vol. 41, no. 8, Dec. 2018, Art. no. e12916.
[33] Y. Zhang and W. Guo, "Moisture content detection of maize seed based on visible/near-infrared and near-infrared hyperspectral imaging technology," *Int. J. Food Sci. Technol.*, vol. 55, no. 2, pp. 631–640, Feb. 2020.
[34] M. Imani and H. Ghassemian, "An overview on spectral and spatial information fusion for hyperspectral image classification: Current trends and challenges," *Inf. Fusion*, vol. 59, pp. 59–83, Jul. 2020.
[35] S. Fan, J. Li, Y. Xia, X. Tian, Z. Guo, and W. Huang, "Long-term evaluation of soluble solids content of apples with biological variability by using near-infrared spectroscopy and calibration transfer method," *Postharvest Biol. Technol.*, vol. 151, pp. 79–87, May 2019.
[36] T. T. Zhang, Y. Y. Xiang, L. M. Yang, J. H. Wang, and Q. Sun, "Wavelength variable selection methods for non-destructive detection of the viability of single wheat Kernel based on hyperspectral imaging," *Spectrosc. Spectral Anal.*, vol. 39, no. 5, pp. 1556–1562, May 2019.
[37] Q. Wang, Y. Liu, Q. Xu, J. Feng, and H. Yu, "Identification of mildew degrees in honeysuckle using hyperspectral imaging combined with variable selection," *J. Food Meas. Characterization*, vol. 13, no. 3, pp. 2157–2166, Sep. 2019.
[38] Y. Lu, W. Wang, M. G. Huang, X. Z. Ni, X. Chu, and C. Y. Li, "Evaluation and classification of five cereal fungi on culture medium using visible/near-infrared (Vis/NIR) hyperspectral imaging," *Infr. Phys. Technol.*, vol. 105, p. 10, Mar. 2020.
[39] C. Xia, S. Yang, M. Huang, Q. Zhu, Y. Guo, and J. Qin, "Maize seed classification using hyperspectral image coupled with multi-linear discriminant analysis," *Infr. Phys. Technol.*, vol. 103, Dec. 2019, Art. no. 103077.
[40] Y. D. Bao, C. X. Mi, N. Wu, F. Liu, and Y. He, "Rapid classification of wheat grain varieties using hyperspectral imaging and chemometrics," *Appl. Sci.-Basel*, vol. 9, no. 19, p. 15, Oct. 2019.
[41] H. Cen and Y. He, "Theory and application of near infrared reflectance spectroscopy in determination of food quality," *Trends Food Sci. Technol.*, vol. 18, no. 2, pp. 72–83, Feb. 2007.
[42] D. Wu, X. Chen, X. Zhu, X. Guan, and G. Wu, "Uninformative variable elimination for improvement of successive projections algorithm on spectral multivariable selection with different calibration algorithms for the rapid and non-destructive determination of protein content in dried laver," *Anal. Methods*, vol. 3, no. 8, pp. 1790–1796, Aug. 2011.
[43] V. Centner, D.-L. Massart, O. E. de Noord, S. de Jong, B. M. Vandeginste, and C. Sterna, "Elimination of uninformative variables for multivariate calibration," *Anal. Chem.*, vol. 68, no. 21, pp. 3851–3858, Jan. 1996.
[44] M. C. U. Araújo, T. C. B. Saldanha, R. K. H. Galvão, T. Yoneyama, H. C. Chame, and V. Visani, "The successive projections algorithm for variable selection in spectroscopic multicomponent analysis," *Chemometric Intell. Lab. Syst.*, vol. 57, no. 2, pp. 65–73, Jul. 2001.
[45] Y. Li, W. Wang, Y. Long, Y. Peng, Y. Li, K. Chao, and X. Tang, "A feasibility study of rapid nondestructive detection of total volatile basic nitrogen (TVB-N) content in beef based on airflow and laser ranging technique," *Meat Sci.*, vol. 145, pp. 367–374, Nov. 2018.
[46] G. Giovanelli, N. Sinelli, R. Beghi, R. Guidetti, and E. Casiraghi, "NIR spectroscopy for the optimization of postharvest apple management," *Postharvest Biol. Technol.*, vol. 87, pp. 13–20, Jan. 2014.
[47] J.-H. Cheng, J.-H. Qu, D.-W. Sun, and X.-A. Zeng, "Visible/near-infrared hyperspectral imaging prediction of textural firmness of grass carp (Ctenopharyngodon idella) as affected by frozen storage," *Food Res. Int.*, vol. 56, pp. 190–198, Feb. 2014.
[48] Y. Y. Zhao, C. Zhang, S. S. Zhu, Y. J. Li, Y. He, and F. Liu, "Shape induced reflectance correction for non-destructive determination and visualization of soluble solids content in winter jujubes using hyperspectral imaging in two different spectral ranges," *Postharvest Biol. Technol.*, vol. 161, p. 11, Mar. 2020.
[49] C. X. Wang, S. L. Wang, X. G. He, and H. Dong, "Detection of saturated fatty acid content in mutton by using the fusion of hyperspectral spectrum and image information," *Spectrosc. Spectral Anal.*, vol. 40, no. 2, pp. 595–601, Feb. 2020.
[50] Q. Wang, Y. Liu, X. Gao, A. Xie, and H. Yu, "Potential of hyperspectral imaging for nondestructive determination of chlorogenic acid content in flos lonicerae," *J. Food Meas. Characterization*, vol. 13, no. 4, pp. 2603–2612, Dec. 2019.
[51] D. Wu, H. Shi, Y. He, X. Yu, and Y. Bao, "Potential of hyperspectral imaging and multivariate analysis for rapid and non-invasive detection of gelatin adulteration in prawn," *J. Food Eng.*, vol. 119, no. 3, pp. 680–686, Dec. 2013.
[52] X. Bai, Q. Xiao, L. Zhou, Y. Tang, and Y. He, "Detection of sulfite dioxide residue on the surface of fresh-cut potato slices using near-infrared hyperspectral imaging system and portable near-infrared spectrometer," *Molecules*, vol. 25, no. 7, p. 1651, Apr. 2020.
[53] W. Guo, F. Zhao, and J. Dong, "Nondestructive measurement of soluble solids content of kiwifruits using near-infrared hyperspectral imaging," *Food Anal. Methods*, vol. 9, no. 1, pp. 38–47, Jan. 2016.
[54] J. Dong and W. Guo, "Nondestructive determination of apple internal qualities using near-infrared hyperspectral reflectance imaging," *Food Anal. Methods*, vol. 8, no. 10, pp. 2635–2646, Nov. 2015.
[55] G. Dong, J. Guo, C. Wang, K. H. Liang, L. G. Lu, J. Wang, and D. Z. Zhu, "Differentiation of storage time of wheat seed based on near infrared hyperspectral imaging," *Int. J. Agricult. Biol. Eng.*, vol. 10, no. 2, pp. 251–258, Mar. 2017.
[56] J. Li, X. Tian, W. Huang, B. Zhang, and S. Fan, "Application of long-wave near infrared hyperspectral imaging for measurement of soluble solid content (SSC) in pear," *Food Anal. Methods*, vol. 9, no. 11, pp. 3087–3098, Nov. 2016.

ZHELI WANG is currently pursuing the master's degree with the College of Mechanical and Electronics Engineering, Shihezi University, Xinjiang, China. He is currently doing research with the Department of Intelligent Detection, Beijing Research Center of Intelligent Equipment for Agriculture, Beijing, China. His current research interests include nondestructive detection and control technology, spectral analysis and imaging processing, and food processing and engineering.

YIFEI ZHANG is currently pursuing the master's degree with the College of Mechanical and Electronics Engineering, Shihezi University, Xinjiang, China. His current research interests include image processing, computer modeling, and the applications of intelligent equipment in agriculture.

SHUXIANG FAN is an Assistant Researcher with the Department of Intelligent Detection, Beijing Research Center of Intelligent Equipment for Agriculture, China. His current research interests include machine learning, imaging and spectral analysis, and the development of intelligent equipment in agriculture.

YINGLAN JIANG is a Researcher with the College of Mechanical and Electronics Engineering, Shihezi University, Xinjiang, China. Her personal research interests are focused on sensing and automation for quality evaluation of fruits, vegetables, and other food products.

JIANGBO LI is an Associate Researcher with the Department of Intelligent Detection, Beijing Research Center of Intelligent Equipment for Agriculture, Beijing, China. He has authored or coauthored over 60 peer-reviewed journal articles in sensing technologies. His personal research interests are focused on sensing and automation for the quality evaluation of fruits, vegetables, and other food products.